Unexpected field-induced dynamics in magnetostrictive microstructured elements under isotropic strain

Simone Finizio,[1,*] Sebastian Wintz,[1,2] Sebastian Gliga,[3] Eugenie Kirk,[1,4] Anna Kinga Suszka,[1,4] Phillip Wohlhüter,[1,4] Katharina Zeissler,[5] and Jörg Raabe[1]

[1]*Paul Scherrer Institut, 5232 Villigen PSI, Switzerland*

[2]*Helmholtz-Zentrum Dresden-Rossendorf, 01328 Dresden, Germany*

[3]*SUPA, School of Physics and Astronomy, University of Glasgow, Glasgow G12 8QQ, United Kingdom*

[4]*Laboratory for Mesoscopic Systems, Department of Materials, ETH Zürich, 8093 Zürich, Switzerland*

[5]*School of Physics and Astronomy, University of Leeds, Leeds LS2 9JT, United Kingdom*

(Dated: June 10, 2018)

Abstract

We investigated the influence of an isotropic strain on the magnetization dynamics of microstructured magnetostrictive $Co_{40}Fe_{40}B_{20}$ (CoFeB) elements with time-resolved scanning transmission x-ray microscopy. We observed that the application of isotropic strain leads to changes in the behavior of the microstructured magnetostrictive elements that cannot be fully explained by the volume magnetostriction term. Therefore, our results prompt for an alternative explanation to the current models used for the interpretation of the influence of mechanical strain on the dynamical processes of magnetostrictive materials.

INTRODUCTION

The magnetostrictive effect describes the influence that the magnetic state of a ferromagnetic material such as Fe or Ni has on its shape. This effect was first reported in 1847 [1], when it was observed that the application of a uniform magnetic field to these materials would cause a mechanical deformation, which manifests either as a compression or as an expansion of the magnetic material. The magnetostrictive effect finds its origins in the spin-orbit coupling mechanism [2], and it can be phenomenologically described as an additional contribution to the magnetic free energy density of the material [2]. The magnitude of the coupling between the magnetic and mechanical responses of these materials is described through the magnetostrictive constant λ_s of the material, typically on the order of 10^{-6} to 10^{-4} [2].

The opposite effect, known as inverse magnetostrictive, or magneto-elastic (ME) coupling effect, describes the response of a magnetostrictive material to a mechanical deformation. A well-known example of the ME effect is given by the uniaxial ME anisotropy generated by the uniaxial straining of a magnetostrictive material, which was observed in many different magnetostrictive systems [2–10]. Under the simplified assumption of a thin film magnetostrictive material where a volume-conserving strain is applied along the plane of the film (i.e. compressive along one axis and tensile along the perpendicular axis), and neglecting the influence of shear strain, the ME anisotropy term can be described as follows [5, 11]:

$$\mathrm{K_{ME}} = -\frac{3}{2}\lambda_s \mathrm{Y} \left|\varepsilon_{xx} - \varepsilon_{yy}\right|, \tag{1}$$

where Y denotes the Young's modulus of the magnetostrictive material, and ε_{ii} the strain applied along the i-th axis. A schematic example of the influence of the ME anisotropy to the magnetic configuration of a microstructured magnetostrictive material is shown in Fig. 1, and experimental verifications of this effect can be found in Refs. [3–9].

Magnetostrictive materials can find applications as an artificial magneto-electric multiferroic composite. Magneto-electric multiferroics are materials exhibiting coupled ferroelectric and ferromagnetic orders. An example of a natural magneto-electric multiferroic, exhibiting ferroelectric and antiferromagnetic orders, is $BiFeO_3$ [12]. The coupling between the ferroelectric and ferromagnetic orders allows e.g. for the control of the spin configuration of the material through the application of an electric field [13, 14]. However due to the rar-

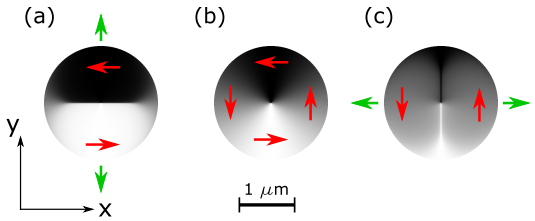

Figure 1. Schematic depiction of the ME coupling effect on a 2 μm diameter disc of a magnetostrictive material with a negative magnetostrictive constant (such as Ni) under (a) an applied tensile strain along the y direction, (b) under no applied strain, and (c) under an applied strain along the x direction. A strain-induced uniaxial ME anisotropy, oriented along the axis perpendicular to the applied tensile strain direction, can be observed. The red arrows indicate the direction of the magnetization in the images, and the green arrows indicate the direction of the applied strain in (a) and (c).

ity of natural multiferroics exhibiting a ferroelectric and ferromagnetic order [15], artificial multiferroic composites, i.e. non multiferroic materials which, combined together, exhibit multiferroic properties, have been an object of attention in recent years. An example of such an artificial multiferroic composite is given by the combination of piezoelectric and magnetostrictive materials, where the application of an electric voltage across the piezoelectric material strains a magnetostrictive material grown on top of the piezoelectric, causing a controllable change in its spin configuration [3–9].

As the ME effect can be phenomenologically described through an additional anisotropy term (given by Eq. (1)) in the magnetic free energy density [2], it is reasonable to expect that the ME effect will also influence the magneto-dynamical response of the magnetostrictive material. This statement is supported both by recent micromagnetic simulations [16–18] and by experimental results [6, 10].

Eq. (1) refers to the case of an anisotropic strain, leading to the generation of a strain-induced ME anisotropy. In the case of an isotropic strain (i.e. $\varepsilon_{xx} = \varepsilon_{yy}$), Eq. (1) yields no uniaxial anisotropy, as expected from symmetry considerations. However, the change in volume caused by the isotropic strain affects the magnetization of the magnetostrictive material through both the volume magnetostriction term and the change in shape of the magnetostrictive element [2]. Such influences can manifest through e.g. a reduction of the saturation magnetization [2]. Similarly to the case of the uniaxial ME anisotropy described in

Eq. (1), the volume magnetostriction term appears in the magnetic free energy, and therefore it is potentially able to influence the magneto-dynamical processes of the magnetostrictive material. However, for most materials, the volume magnetostriction term ω is several orders of magnitude lower than the magnetostrictive constant λ_s leading, under otherwise equal conditions, to much smaller responses of the magnetostrictive material to isotropic strains [2]. Therefore, it is expected, for small isotropic strains, that the magnetostrictive material will not exhibit sizable modifications in its magneto-dynamical behavior.

In the work presented here, we experimentally investigate the influence of a static isotropic strain on the gyration dynamics of magnetic vortices stabilized in microstructured CoFeB elements. The microstructured elements were strained by bending the square Si_3N_4 membrane on which they were fabricated, as described in Ref. [19]. The magnetic vortices were excited with a magnetic field pulse, and the gyration dynamics were recorded by time-resolved scanning transmission x-ray microscopy (STXM) imaging. Unexpectedly, we observed a decrease of the vortex gyration eigenfrequency with the applied strain which cannot be explained by solely considering the contributions arising from the volume magnetostriction and form factor terms.

EXPERIMENTAL

Microstructured elements of different geometries fabricated out of Ni and CoFeB, both of which are magnetostrictive, albeit with opposite signs of the magnetostrictive constant, were patterned by electron beam lithography with lift-off step on top of 50 nm thick Si_3N_4 membranes with square and rectangular geometries, and by an ion milling step on 100 nm thick square Si_3N_4 membranes.

For the lift-off step process, a bi-layer of methyl-methacrylate (MMA) and of poly-methyl-methacrylate (PMMA) was spin-coated on top of the Si_3N_4 membranes before the lithographical exposure, which was carried out with a Vistec EBPG 5000Plus electron beam writer. The energy of the electrons was tuned to 100 keV, and a writing dose of 1800 μC cm^{-2} was employed. To reduce the influence of charging during the exposure, a 7 nm thick layer of Al was deposited using a Balzers BAE250 thermal evaporator. After the exposure, the Al layer was removed by immersion in tetramethyl-ammonium-hydroxide followed by rinsing in deionized water. Following the removal of the Al charge drain layer, the exposed resist

was developed by immersion for 120 s in a solution of methyl-isobutyl-ketone and isopropyl alcohol 1:3 in volume, and subsequent immersion for 60 s in pure isopropyl alcohol. The Ni films were deposited at a thickness of 25 nm by thermal evaporation using a Leybold L560 evaporator with a base pressure of the order of 10^{-6} mbar at a growth rate of 30 nm min^{-1}. The CoFeB films were grown to a thickness between 25 and 50 nm by DC sputtering in a dedicated sputtering system with a base pressure of the order of 10^{-8} mbar at a growth rate of 1.7 nm min^{-1}. Following the growth of the films, the unexposed resist was removed, along with the metal film on top of it, by immersion in pure acetone.

For the ion-milling step, 50 nm CoFeB films were deposited by DC sputtering on top of the membrane, and a layer of MAN-2410 resist was spin coated on top of the CoFeB film, and exposed with a 10 keV electron beam. An Ar ion milling step was then employed to define the CoFeB microstructures. After the ion milling, the remaining resist was removed by immersion in acetone.

To excite the magnetostrictive microstructures, Cu striplines were fabricated on top. Such striplines allow for the generation of a pulsed in-plane magnetic field by injecting an electrical current across the stripline. To fabricate the striplines, a bi-layer of MMA and PMMA was spin-coated on top of the sample, and exposed using electron beam lithography with an electron energy of 100 keV and an exposure dose of 1500 $\mu\text{C cm}^{-2}$. Similarly to the exposure of the magnetostrictive microstructures, a 7 nm thick Al charge drain layer was deposited on top of the resist to prevent charging during the exposure. Au registration markers guaranteed the correct alignment between the magnetostrictive microstructures and the Cu stripline. To develop the exposed resist, the same process used for the magnetostrictive microstructures was employed. Finally, a Cu film was deposited using a Balzers BAE250 thermal evaporator, and the unexposed resist removed along with the metal film on top of it by immersion in pure acetone.

A scanning electron micrograph of one of the fabricated samples, showing the magnetostrictive microstructures and the Cu stripline fabricated on top of the Si_3N_4 membrane is shown in Fig. 2.

The field-induced magneto-dynamical processes were imaged by time-resolved STXM at the PolLux endstation (X07DA) of the Swiss Light Source [20] in the pump-probe scheme. A Fresnel zone plate with an outermost zone width of 25 nm was employed for focusing circularly-polarized x-rays on the sample. The entrance and exit slits to the monochromator

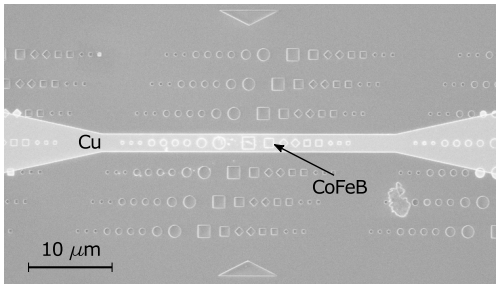

Figure 2. Scanning electron micrograph of microstructured CoFeB elements with different geometries fabricated on top of a 50 nm thick Si_3N_4 membrane. To excite the microstructures, a Cu stripline was fabricated on top of the microstructured elements.

were selected to guarantee an x-ray beam spot on the order of 30 nm, as a compromise between spatial resolution and photon flux. Magnetic contrast was achieved through the x-ray magnetic circular dichroism (XMCD) effect. To allow for the imaging of the in-plane component of the magnetization, the samples were mounted with their surface normal oriented at 30° with respect to the x-ray beam. The images were then scaled with a factor of $2/\sqrt{3}$ in the x direction to compensate for the 30° orientation.

To strain the magnetostrictive microstructured elements, the Si_3N_4 membranes were mechanically bent by a pressure difference between the two sides of the membrane. This is achieved, as described in detail in Ref. [19], with a pressurized environmental gas cell where the membrane is integrated in the sealing element. Depending on the geometry of the membrane, isotropic or anisotropic mechanical strains can be generated on the magnetostrictive microstructures [19].

Particular attention needs however to be dedicated to the Cu stripline fabrication, in particular to its thickness. The presence of a thick Cu stripline influences the local bending of the membrane, causing a modification of the mechanical strain applied to the magnetostrictive elements with respect to the model described in Refs. [19, 21]. As shown in Fig. 3, the thickness of the Cu stripline plays a critical role in the strain that can be generated by bending the Si_3N_4 membrane: a thick stripline is preferred for time-resolved experiments, as it allows both for the injection of higher electrical currents, and for the efficient removal of the heat generated by the electrical current. However, as shown in Fig. 3(a-b), a thick stripline hinders the straining of the magnetostrictive microstructures. Therefore, a compromise between bending and heat dissipation, depending on the geometry and thickness

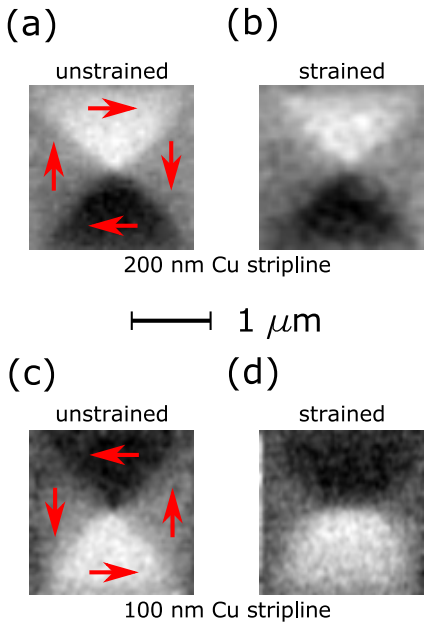

Figure 3. Influence of the stripline thickness on the strain generated by bending a 50 nm thick Si_3N_4 membrane on a 2 μm wide CoFeB microstructured square. (a-b) Thick (about 200 nm) Cu stripline. (c-d) Thinner (about 100 nm) Cu stripline. Images (a) and (c) show the magnetic configuration of the CoFeB square in the absence of applied strain (stabilizing a symmetric Landau flux closure pattern), while images (b) and (d) show the magnetic configuration of the square under an applied pressure difference of 600 mbar between the two sides of the membrane. A ME anisotropy can be observed for image (d), indicating that the CoFeB microstructure is being strained by the membrane bending, while image (b) still shows a symmetric Landau pattern, indicating that the thick Cu stripline is hindering the straining of the CoFeB microstructured element. The red arrows indicate the direction of the magnetization.

of the membrane, needs to be found. For the case of a 50 nm thick Si_3N_4 membrane, the best compromise was found for a Cu thickness of 100 nm, as shown in Fig. 3(c-d). Instead, for the case of a 100 nm thick Si_3N_4 membrane, the best compromise was found for a Cu thickness of about 200 nm.

For membranes with a rectangular geometry, the bending of the membrane leads to the generation of a uniaxial ME anisotropy for both the Ni and CoFeB microstructured elements [10, 19], given by Eq. (1).

Ni and CoFeB exhibit an opposite sign for their magnetostrictive constant λ_s [2, 22] meaning that, under equal conditions, the sign of the uniaxial magnetostrictive anisotropy given

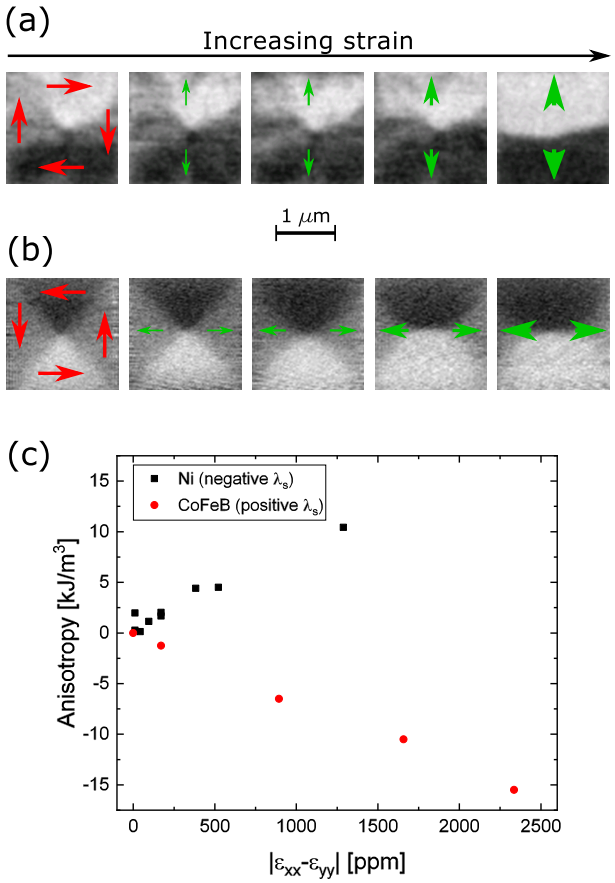

Figure 4. Spin configuration of (a) a 2 μm Ni and of (b) a 2 μm CoFeB (both 25 nm thick) microstructured square fabricated on top of a rectangular Si_3N_4 membrane under an increasing applied uniaxial strain. A uniaxial ME anisotropy is generated by the mechanical straining of the microstructured elements through the bending of the membrane. The red arrows in the figure indicate the direction of the magnetization in the images, and the green arrows indicate the direction of the tensile strain generated by the bending of the membrane. Note here that the strain in (a) is oriented at 90 degrees with respect to the strain in (b). Due to the opposite sign of the magnetostrictive constant of Ni and CoFeB, the strain-generated ME anisotropy is oriented differently for the two magnetostrictive materials, as shown in (c), where the magnitude of the ME anisotropy as a function of the strain generated by the bending of the membrane is shown.

by Eq. (1) will be opposite for the two materials. This is shown in Fig. 4. The magnitude of the uniaxial ME anisotropy generated by the straining of the microstructured elements can be estimated, as described in Ref. [3], by comparing the magnetic microscopy images with micromagnetic simulations, as shown in Fig. 4(c). The micromagnetic simulations

were carried out with the MuMax^3 framework [23].

It is worth to note here that the selection of the magnetostrictive material plays an important role in the experimental investigation of the magneto-dynamical contributions of the ME effect. In particular, as shown in Fig. 4, the Ni microstructured elements exhibit a strong signature of the influence of both a pre-existing magneto-crystalline anisotropy and of pinning, which is manifesting itself particularly clearly in the shape of the domain walls stabilized in the microstructured square shown in Fig. 4(a). Converseley, the CoFeB microstructured elements, shown in Fig. 4(b), exhibit a magnetic configuration determined by the shape anisotropy, without the influence of pre-existing magneto-crystalline anisotropies or arising from pinning sites, therefore allowing for an easier investigation of the influence of the ME anisotropy, and to identify the dynamical processes more clearly. Therefore, the experiments presented here will focus on the CoFeB microstructured elements.

To excite the gyration dynamics of the magnetic vortices, a 5 ns long electrical current pulse was injected across the stripline. This generates an in-plane magnetic field pulse (with an amplitude on the order of 5 mT), which causes the displacement of the magnetic vortex stabilized at the center of the microstructure. After the magnetic field pulse, the magnetic vortex relaxes back to its equilibrium position via a gyrotropic motion. The gyration dynamics was probed using the x-ray flashes generated by the synchrotron light source as probing signal, using a dedicated field-programmable gate array setup combined with a fast avalanche photodiode as x-ray detector, which also provides the timing and synchronization signals that guarantee that the pump signal is synchronized with the 500 MHz master clock of the synchrotron light source [24]. The temporal resolution for the experiments presented here was 200 ps.

The eigenfrequency of the gyrotropic motion of the magnetic vortices was determined from the time-resolved STXM images (see the supplementary information for an example of the time-resolved STXM images employed in the work described here) by fitting the time-resolved XMCD contrast variation with an exponentially damped sinusoid, as described in detail in Ref. [10].

RESULTS AND DISCUSSION

The influence of a uniaxial strain on the dynamical processes of magnetostrictive microstructures was already investigated in previous works [6, 10, 16]. Therefore, in the work presented here, we will concentrate on the case of an isotropic strain, i.e. on the microstructured elements fabricated on top of Si_3N_4 membranes with square geometry. In particular, 500 μm wide square Si_3N_4 membranes were employed for the straining of the magnetostrictive microstructures.

A 2.5 μm CoFeB diameter disc (see left side of Fig. 2), fabricated at the center of the square membrane, and stabilizing a vortex state in the absence of applied strain, was investigated. A magnetic field pulse, generated according to the protocol described in the previous section, was employed to excite the gyration of the magnetic vortex. To compare the results with the case of an applied uniaxial strain described in Ref. [10], the measurements were focused on the determination of the vortex core gyration eigenfrequency as a function of the applied strain.

The gyration eigenfrequency as a function of the applied isotropic strain for the 2.5 μm diameter disc extracted from the time-resolved images is shown in Fig. 5. The magnitude of the applied isotropic strain was determined from the measured pressure difference between the two sides of the square Si_3N_4 membrane employing the equations given in Refs. [19, 21].

A decrease of the vortex gyration eigenfrequency with the applied isotropic strain, similar to the results reported in Ref. [10], can be observed for the 2.5 μm diameter disc. The reduction of the gyration eigenfrequency for the 2.5 μm diameter disc could in principle be explained by a reduction of the saturation magnetization due to the contribution of the volume magnetostriction term, due to the linear dependence of the vortex gyration eigenfrequency with the saturation magnetization appearing in the Thiele equation [25]. However, the change in the saturation magnetization necessary to justify the measured changes in the gyration eigenfrequency is too large to find its origin in the volume magnetostriction term. This is due to the negligible value of the volume magnetostrictive constant ω for materials such as Ni and CoFeB, which are on the order of $\omega \simeq 10^{-11}$, with respect to the magnetostrictive constant λ_s, which is on the order of $\lambda_s \simeq 10^{-5}$ for these materials [2]. A uniaxial ME anisotropy could explain the observed results for the 2.5 μm disc, as the changes in the gyration eigenfrequency are comparable in magnitude to the results reported in Ref. [10].

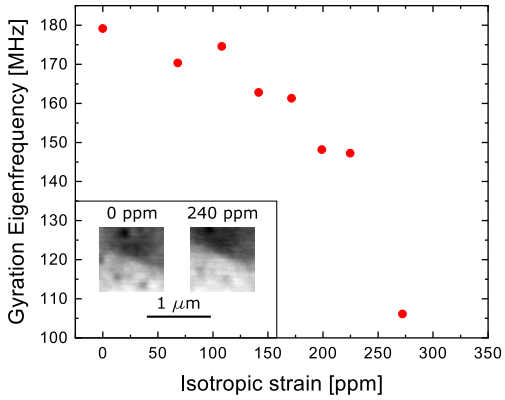

Figure 5. Vortex gyration eigenfrequency in a 2.5 μm diameter CoFeB disc fabricated on top of a square Si_3N_4 membrane as a function of an applied isotropic strain. A reduction of the gyration eigenfrequency with the applied strain can be observed. The inset shows static XMCD-STXM images of the center of the disk at no applied strain and at an applied isotropic strain of about 240 ppm. No clearly detectable changes in the magnetic domain structure can be observed upon the application of the isotropic strain.

However, due to the geometry of the membrane, and to the fact that no substantial changes of the static magnetic configuration of the CoFeB microstructured discs were observed when changing the applied strain, this explanation is also not correct. Finally, micromagnetic simulations show that the experimentally-induced geometric curvature of the sample following the bending of the Si_3N_4 membrane does not affect the small amplitude gyration eigenfrequency of the vortex.

The results presented here cannot therefore be explained by merely considering the volume magnetostriction or the changes in the shape of the magnetic microstructures [2], and no contribution due to the uniaxial ME anisotropy is expected for the experiments presented here, due to the geometry of the membrane. Our results require an alternative explanation to the current models used for the interpretation of the influence of a mechanical strain on the dynamical processes of magnetostrictive materials. Recently, non-Joulian magnetostrictive effects have been observed on Fe_xGa_{1-x} magnetostrictive alloys [26]. Further investigations will be required to discover whether the changes in the dynamical behavior of the magnetostrictive microstructures reported in the work can be explained as a non-Joulian magnetostrictive effect.

CONCLUSIONS

In conclusion, we have investigated the gyration of magnetic vortices in magnetostrictive CoFeB microstructured elements under an applied isotropic strain, generated by bending a Si_3N_4 membrane with a square geometry. Albeit no significant changes of the vortex gyration dynamics are expected for an isotropic strain, due to the small magnitude of the volume magnetostrictive constant of CoFeB, we observed, unexpectedly, a significant change of the vortex gyration eigenfrequency with the applied isotropic strain, which still requires an alternative explanation to the current model used for the description of the influence of an isotropic strain on the magneto-dynamical processes of magnetostrictive materials.

Part of this work was performed at the PolLux (X07DA) endstation of the Swiss Light Source, Paul Scherrer Institut, Villigen, Switzerland. The authors would like to thank B. Sarafimov and A. Weber for technical support, R. Mattheis for the deposition of the CoFeB films, and the nanopatterning facilities at the Laboratory for Micro and Nanotechnology at PSI and at the Ion Beam Center at HZDR for the fabrication of the samples. The research leading to these results has received funding from the European Community's Seventh Framework Programme (FP7/2007-2013) under grant agreement No. 290605 (PSI-FELLOW/COFUND), and the European Union's Horizon 2020 Project MAGicSky (Grant No. 665095). The PolLux endstation was financed by the German Minister für Bildung und Forschung (BMBF) through contracts 05KS4WE1/6 and 05KS7WE1. SG was funded by the European Union's Horizon 2020 Research and Innovation Programme under the Marie Sklodowska-Curie grant agreement No. 708674.

* Corresponding Author: simone.finizio@psi.ch

[1] J. P. Joule, The London, Edinburgh and Dublin Philosophical Magazine and Journal of Science **30**, 76 (1847).

[2] E. W. Lee, Reports on Progress in Physics **18**, 184 (1955).

[3] S. Finizio, M. Foerster, M. Buzzi, B. Krüger, M. Jourdan, C. Vaz, J. Hockel, T. Miyawaki, A. Tkach, S. Valencia, F. Kronast, G. Carman, F. Nolting, and M. Kläui, Physical Review Applied **1**, 021001 (2014).

[4] M. Buzzi, R. V. Chopdekar, J. L. Hockel, A. Bur, T. Wu, N. Pilet, P. Warnicke, G. P. Carman, L. J. Heyderman, and F. Nolting, Physical Review Letters **111**, 027204 (2013).

[5] M. Weiler, A. Brandlmaier, S. Geprägs, M. Althammer, M. Opel, C. Bihler, H. Huebl, M. S. Brandt, R. Gross, and S. T. B. Goennenwein, New Journal of Physics **11**, 013021 (2009).

[6] M. Foerster, F. Macia, N. Statuto, S. Finizio, A. Hernandez-Minguez, S. Landinex, P. V. Santos, J. Fontcuberta, J. Manel Hernandez, M. Kläui, and L. Aballe, Nature Communications **8**, 407 (2017).

[7] T. Wu, P. Zhao, M. Bao, A. Bur, J. Hockel, K. Wong, K. Mohanchandra, C. Lynch, and G. Carman, Journal of Applied Physics **109**, 124101 (2011).

[8] J. L. Hockel, A. Bur, T. Wu, K. P. Wetzlar, and G. P. Carman, Applied Physics Letters **100**, 022401 (2012).

[9] J. Cui, C. Y. Liang, A. Paisley, A. Sepulveda, J. F. Ihlefeld, G. P. Carman, and C. S. Lynch, Applied Physics Letters **107**, 092903 (2015).

[10] S. Finizio, S. Wintz, E. Kirk, A. K. Suszka, S. Gliga, P. Wohlhüter, K. Zeissler, and J. Raabe, Physical Review B **96**, 054438 (2017).

[11] A. Brandlmaier, S. Geprägs, M. Weiler, A. Boger, M. Opel, H. Huebl, C. Bihler, M. S. Brandt, B. Botters, D. Grundler, R. Gross, and S. T. B. Goennenwein, Physical Review B **77**, 104445 (2008).

[12] G. Catalan and J. F. Scott, Advanced Materials **21**, 2463 (2009).

[13] M. Fiebig, Journal of Physics D: Applied Physics **38**, R123 (2005).

[14] N. Spaldin and M. Fiebig, Science **309**, 391 (2005).

[15] N. Hill, Journal of Physical Chemistry B **104**, 6694 (2000).

[16] D. E. Parkes, R. Beardsley, S. Bowe, I. Isakov, P. A. Warburton, K. W. Edmonds, R. P. Campion, B. L. Gallagher, A. W. Rushforth, and S. A. Cavill, Applied Physics Letters **105**, 062405 (2014).

[17] P. Roy, Applied Physics Letters **102**, 162411 (2013).

[18] T. A. Ostler, R. Cuadrado, R. W. Chantrell, A. W. Rushforth, and S. A. Cavill, Physical Review Letters **115**, 067202 (2015).

[19] S. Finizio, S. Wintz, E. Kirk, and J. Raabe, Review of Scientific Instruments **87**, 123703 (2016).

[20] J. Raabe, G. Tzvetkov, U. Flechsig, M. Böge, A. Jaggi, B. Sarafimov, M. Vernooij, T. Huthwelker, H. Ade, D. Kilcoyne, T. Tyliszczak, R. Fink, and C. Quitmann, Review of Scientific Instruments **79**, 113704 (2008).

[21] W. K. Schomburg, *Introduction to Microsystem Design* (Springer Verlag, 2011).

[22] D. Wang, C. Nordman, Z. Qian, J. M. Daughton, and J. Myers, Journal of Applied Physics **97**, 10C906 (2005).

[23] A. Vansteenkiste, J. Leliaert, M. Dvornik, M. Helsen, F. Garcia-Sanchez, and B. Van Waeyenberge, AIP Advances **4**, 107133 (2014).

[24] A. Puzic, T. Korhonen, B. Kalantari, J. Raabe, C. Quitmann, P. Jüllig, L. Bommer, D. Goll, G. Schütz, S. Wintz, T. Strache, M. Körner, D. Marko, C. Bunce, and J. Fassbender, Synchrotron Radiation News **23**, 26 (2010).

[25] A. Thiele, Physical Review Letters **30**, 230 (1974).

[26] H. D. Chopra and M. Wuttig, Nature **521**, 340 (2015).